Spectrochimica Acta Part B: Atomic Spectroscopy 189 (2022) 106367

Contents lists available at ScienceDirect

Spectrochimica Acta Part B: Atomic Spectroscopy

journal homepage: www.elsevier.com/locate/sab

Microliter-stirred sample setup for X-ray spectroscopy analysis of nanomaterials in suspension

Rafał Fanselow [a,*], Anna Wach [a,b], Wojciech Błachucki [a], Jakub Szlachetko [a,*]

[a] Institute of Nuclear Physics Polish Academy of Sciences, Radzikowskiego 152, Cracow 31-342, Poland
[b] Paul Scherrer Institut, CH-5232 Villigen PSI, Switzerland

ARTICLE INFO

Keywords:
Nanomaterial suspension
Sample setup
Agglomeration
Sedimentation
X-ray spectroscopy

ABSTRACT

Analysis of samples in the liquid environment using X-ray spectroscopy techniques is a very attractive approach as it provides specimen characterization in its native conditions thanks to the penetrating properties of X-rays. However, very often due to challenging synthesis procedures and the high cost of specimens it is difficult to obtain a sample in quantities for optimal measurement. Additionally, nanoparticles (NPs) aqueous suspensions are often not stable and undergo agglomeration and sedimentation processes that can be avoided either by sonication or sample stirring. Relatively small sample volumes and intrinsic agglomeration processes make X-ray spectroscopy measurements challenging especially when long periods are needed for the collection of high-quality data. To address both issues, we developed dedicated sample system that allows measurements down to few tens of μL of the liquid sample with capability of continuous stirring of the suspension. The X-ray spectroscopy measurements of ZnO nanoparticles suspension in water showed a stable signal for hours of acquisition time. On the other hand, in the absence of stirring, agglomeration and subsequent sedimentation processes were visible already within few minutes with maximum sedimentation rate of 2.5% of concentration loss in the beam field per minute.

1. Introduction

Nanotechnology is a very rapidly growing multidisciplinary field of science applied in numerous areas both at the high-tech and general-purpose level [1,2]. It focuses on nanomaterials typically defined as objects with characteristic dimensions below 100 nm whose size-dependent properties are driven by quantum phenomenons [3]. To fully understand and control nanomaterial's behavior, a proper qualitative and quantitative assessment of their characteristics is necessary, preferably in their native environment for example in the form of liquid suspensions.

Nowadays, researchers have access to various analytical techniques to probe suspended nanoobjects. For example, size distributions of nanomaterials in a liquid environment could be obtained by utilizing light scattering methods like Dynamic Light Scattering (DLS) or Nanoparticle Tracking Analysis (NTA) [4,5]. While being useful in deriving dimensions of the nanostructures, these kinds of techniques do not give information about other properties of the sample. UV-VIS spectroscopy is another widely used method to characterize nanomaterial dispersions. The application of optical probing involves chromophore detection and exploration of phenomenons specific to nanoscale objects such as localized surface plasmon resonance (LSPR) in metallic nanoparticles and quantum confinement effect in semiconductor quantum dots [6,7]. However, many materials do not give any characteristic signal in the visible or near-ultraviolet part of the electromagnetic spectrum and therefore cannot be identified and examined by UV-VIS spectroscopy. Moreover, the optical analysis does not give the full view of the electronic structure of the samples, thus creating a demand for other experimental approaches to fulfill the information gap about the specimen.

X-ray spectroscopy provides an element-specific, bulk-sensitive and non-destructive tool to probe the electronic structure of the samples in ambient conditions owing to the penetrating properties of X-rays [8]. Bright synchrotron sources complemented with the recently developed laboratory setups for routine day-to-day experiments make a study of nanosuspensions involving X-ray absorption spectroscopy (XAS) and X-ray emission spectroscopy (XES) available for scientists more than ever before [9,10]. However, analysis of nanomaterials in solutions often proves to be problematic. This is mainly because many novel nanosystems have complex synthetic procedures and the high cost of

* Corresponding authors.
E-mail addresses: rafal.fanselow@ifj.edu.pl (R. Fanselow), jakub.szlachetko@ifj.edu.pl (J. Szlachetko).

https://doi.org/10.1016/j.sab.2022.106367
Received 8 September 2021; Received in revised form 29 December 2021; Accepted 13 January 2022
Available online 18 January 2022

ingredients, which makes it difficult to prepare in sufficient quantities for optimal measurement [11,12]. Another limiting factor originates from nanoparticles' natural tendency to attract each other to form bigger structures in a process called agglomeration [13,14]. Weak van der Waals interactions and nanomaterials' high surface energy results in the formation of loosely bounded clusters [15–17]. Agglomeration is known to significantly alter the nanosuspensions' properties compared to well-dispersed nanoparticles [18–20]. Moreover, as the size of growing agglomerates in the fluid increases, the gravitational force acting on the particles becomes more dominant and eventually overcomes Brownian diffusion leading to sedimentation, i.e., settlement of particles at the bottom of the container [21]. Depending on various aspects related to the suspended objects (size, shape, density, concentration, surface charge, and other surface modifications) and the solvent (viscosity, density, pH) as well as the possible addition of other substances like surfactants, sedimentation may occur on the timescales from several weeks to even few minutes [22–30]. Agglomeration and sedimentation of the nanoparticles become a serious challenge that needs to be addressed before attempting to analyze such samples [4]. The most commonly applied procedure of achieving the nanosuspension's stability involves its pre-treatment via either mechanical mixing, intensive shaking or ultrasonication before the measurement [31]. Despite differences in their performance, principally, the mechanism of action is similar for all three approaches: energy delivered to the system breaks down the agglomerates into smaller particles and at the same time temporarily disperses them evenly within the solvent. Nevertheless, the deagglomerated nanomaterials are afterwards still prone to re-agglomeration since neither of the mentioned strategies changes the overall interaction balance of the sample solution [32]. Therefore, for measurements requiring a long time of data collection nanoparticle suspension needs to be constantly perturbed during signal acquisition to obtain high-quality results. Unfortunately, most of the commercially available laboratory instruments intended for the analysis of liquid samples are not adapted for continuous mixing of low sample volumes. Simultaneously, such a system should also provide a sufficient amount of space as well as accessibility in the immediate sample environment allowing to implement X-ray spectroscopy methods to probe the nanomaterial.

To address issues associated with the examination of nanostructures in solutions, herein, we report a recently developed microliter-stirred sample setup designed to characterize very low amounts of nanomaterial suspensions of down to 50 μL with sustained sample mixing successfully preventing particle agglomeration and sedimentation. Our custom-made system was installed at a laboratory double X-ray spectrometer and tested with 200 mM zinc oxide nanoparticle dispersion using simultaneous XAS and XES measurements. A series of conducted experiments with and without applied mechanical stirring showed the crucial role of the designed setup in the acquisition of high-quality Zn K-edge XAS and Zn Kα XES spectra. In summary, we demonstrate that the use of X-ray spectroscopy allows for in situ, element-specific, quantitative investigations of ZnO NPs and determination of NPs agglomeration and sedimentation rates.

2. Experimental

2.1. Microliter-stirred sample setup

The designed sample setup is depicted in Fig. 1a) and 1b) in form of a schematic drawing and a photograph of the setup as installed for laboratory X-ray measurements. The system consists of 3 major parts: the microliter liquid sample container, a stirring device and a holder which allowed mounting both elements and fixing them to the sample positioning system. A capillary made of polyimide (Kapton, from Goodfellow) was used as a vessel for nanomaterial solution whose chemical resistance and transparency to X-rays make it ideal for these purposes. We should note however, that other materials can be used depending on

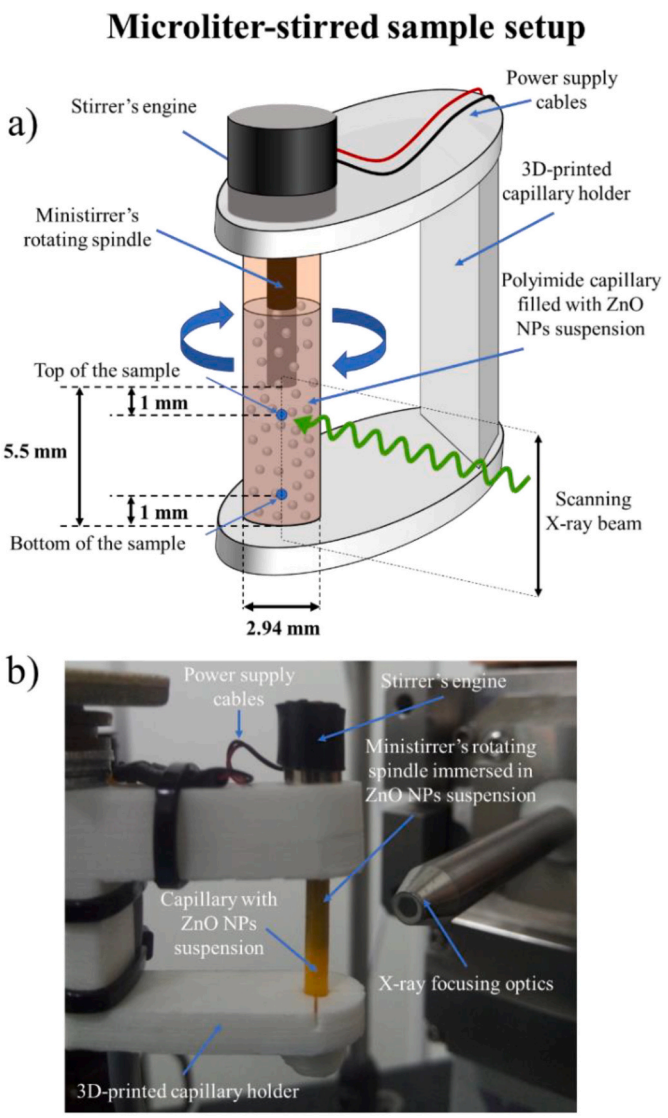

Fig. 1. Microliter-stirred sample setup: a) schematical drawing with the distinction of the individual elements and the area irradiated by X-ray beam b) photograph of the setup taken in the laboratory.

specific experimental requirements and the needed chemical resistivity of the container. The tube's inner diameter of 2.94 mm was chosen to achieve sufficient pathlength for incoming photons while minimizing the amount of specimen necessary for the analysis. The bottom end of the capillary was plugged with a 3D-printed polylactide (PLA) stopper and sealed with parafilm to avoid any potential leakage of the fluid. To ensure the sample's stability during long-time measurements, a miniature electric engine (manufacturer: OEM, model: MT51) was implemented. The device was equipped with a thin spindle covered with protective polyvinyl chloride (PVC) coating. When the external voltage of up to 3 V is applied the spindle immersed in the dispersion rotates perturbing the dispersed particles to avoid their agglomeration. The volume of the sample was set at 150 μL to ensure enough area (about 5.5 mm in height) to probe sedimentation and agglomeration processes with the X-ray signals measured at different height positions. However, a shorter capillary can be employed and sample volumes as low as few tens of μL can be examined.

2.2. Experiment with laboratory double X-ray spectrometer setup

Simultaneous Zn K-edge XAS and Zn Kα XES measurements were

performed using laboratory setup based on two von Hámos geometry X-ray spectrometers schematically presented in Fig. 2. The whole system is described in detail in [33]. Briefly, laboratory setup is composed of the X-ray source (XOS X-beam Superflux PF X-ray tube with Mo anode) with focusing optics providing around 100 × 100 μm^2 X-ray spot at the sample position and two independent X-ray spectrometer layouts: one for the detection of transmitted photons through the sample (XAS) and the other for collection of emitted characteristic X-rays (XES). Both configurations utilize cylindrically bent analyzer crystal of 25 cm radius of curvature which Bragg-diffracts photons along one axis and focuses them in the direction of the second axis. According to the Bragg's law, the radiation diffracted by the crystal is directed to the detector (Andor Newton DO920P) equipped with a front-illuminated CCD camera consisting of 1024 × 256 pixels with 26 μm size each. The crystals used in the experiments were Si(800) and Si(444) for the measurements of Zn K-edge XAS and Zn Kα XES spectra, respectively. The sample setup with stirred nanosuspension was installed at a motorized platform with three micrometer positioners allowing for sample alignment in vertical, horizontal axes and along the incoming incident beam.

The microliter-stirred sample setup was tested using zinc oxide nanoparticle (NP) dispersion (20% wt.) of the average size of 40 nm in distilled water (obtained from Sigma-Aldrich). The suspension was diluted from basic concentration to 200 mM. The XAS and XES measurements were performed with the X-ray tube's voltage and current set to 30 kV and 0.9 mA and the detectors' chips cooled to −40 °C. The voltage applied to the stirrer was 0.6 V. X-ray beam was focused at the middle of the capillary in the horizontal direction, perpendicular to the X-ray beam. In the vertical direction, two spots marked in Fig. 1a) have been chosen for data collection: one 1 mm below the stirrer's spindle and another 1 mm above the 3D-printed capillary holder. In the next parts of the article, these two positions will be referred to as “top” and “bottom” of the sample, respectively. The measurements were done at top and bottom positions with the stirrer turned off and on, resulting in 4 series of data obtained in total. At each of the 4 conditions mentioned, a series of 20 4.4-min simultaneous XAS and XES measurements were done to allow analysis of the potential time-dependent signal changes that could be attributed to agglomeration and sedimentation processes. The chosen timestep value was a compromise between achieving sufficient time resolution of the measurement and providing good statistics of the detected X-ray signals.

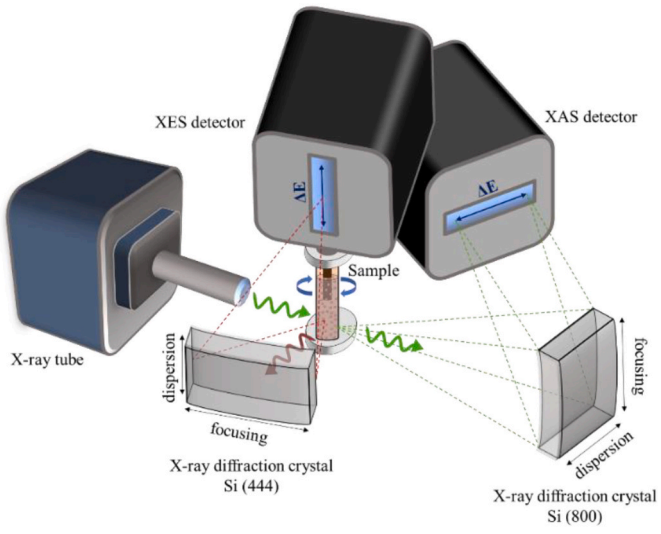

Fig. 2. Schematical representation of experimental setup for simultaneous XAS and XES measurements.

3. Results and discussion

3.1. XES & XAS spectral dependences on ZnO NPs concentration

Fig. 3a) and 3b) present the reference Zn Kα XES and Zn K-edge XAS spectra, respectively, measured for 200 mM ZnO NPs suspension with the laboratory setup. The data was obtained by summing two full datasets of measurement at top and bottom of the sample with applied mechanical stirring. The clearly visible on the XES spectrum $K\alpha_1$ and $K\alpha_2$ emission peaks are attributed to electronic transitions from $2p_{3/2}$ (~8640 eV and 3.45 eV FWHM) and $2p_{1/2}$ (~8616 eV with 3.64 eV FWHM) states to the core 1 s level. The FWHM values were obtained by fitting the Voigt function (blue line) to the experimental data (red points). The Voigt FWHM originates from the convolution of a Gaussian component determining the energy resolution of the X-ray spectrometer and the Lorentzian component characterizing the natural widths of X-ray emission lines. From the fit we obtained experimental resolution of 1.6 (±0.13) eV and the Lorentzian $K\alpha_1$ and $K\alpha_2$ widths of 2.67 (±0.10) eV and 2.89 (±0.12) eV, respectively. The acquired values are slightly larger than the tabulated values of 2.3 eV for $K\alpha_1$ and 2.68 eV for $K\alpha_2$ [34]. This discrepancy may result from our simple one-peak fitting to each of the measured Kα lines. It is also important to note that due to the extended source along the primary beam direction the actual beam size on the sample varies by the amount of +10% at the entrance and the exit of the capillary as compared to the spot size at the focusing point of the X-ray optics. As a result, one may expect the overall resolution for the thin sample to be a few percent better than obtained 1.6 eV. We should note that the resolution of the setup doesn't change linearly with the sample thickness because the total spectrometer resolution is given by a convolution of several quantities that includes detector's and diffraction crystal parameters and geometrical effects.

The XAS Zn K-edge spectrum was acquired by processing measured transmittance data using Lambert-Beer Law. The obtained data (brown points) agrees with the synchrotron spectrum (yellow line) measured at a similar concentration of ZnO NPs [35]. The main features of the XAS Zn K-edge spectrum that give information about the unoccupied energy states of the element can be easily identified. The transition at around 9666 eV, just above absorption edge (~9664 eV), is associated with excitation of the 1 s electron to the 4p state and is observed on the K-edge XAS spectra of many transition metals compounds. Higher above it, there are two peaks, including the main maximum at ~9671 eV and one at ~9682 eV, corresponding to photons with the energy exceeding the ionization potential of zinc K-edge electrons and related to the appearance of the photoelectron waves scattered on nearby atoms [36]. Small differences in the intensity of the abovementioned features relative to the reference spectrum are likely caused by the resolution abilities of the laboratory XAS spectrometer.

In order to monitor and evaluate the effects of potential agglomeration and sedimentation of the ZnO nanoparticles during the experiment, we defined the parameters derived from XAS and XES data that give direct information about the amount of specimen in the path of the incoming X-ray beam. Since the obtained XES signal is proportional to the sample concentration [37], the selected quantity of interest was simply the total number of photon counts recorded by the detector in the energy range of $K\alpha_1$ and $K\alpha_2$ emission lines as presented in Fig. 4a). The energy range of photon integration was around 50 eV, which corresponds approximately to 300 pixels on the CCD camera.

Fig. 4b) shows the transmittance spectrum through ZnO NPs suspension. The XAS spectra were obtained by processing the experimental data through the Lambert-Beer law. The relative decrease and increase of ZnO nanoparticles concentration would mainly be visible as the changes in logarithm of the ratio of pre-edge and post-edge intensities in the transmittance spectrum denoted in the Fig. 4b) as blue and red solid lines. The transmittance spectra were normalized by I_0 spectrum.

To correlate the discussed parameters with ZnO NPs concentration, we performed XES and XAS calibration measurements. The

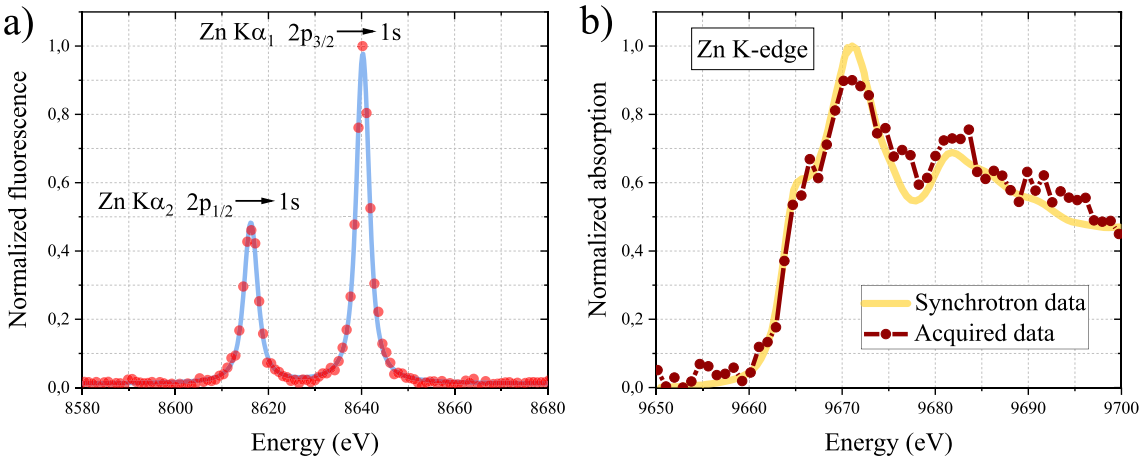

Fig. 3. X-ray spectroscopy spectra collected for 200 mM ZnO nanoparticle suspension with applied microliter-stirred sample setup: a) Zn Kα XES spectrum (red points) with fitted Voigt function (blue line) to $K\alpha_1$ and $K\alpha_2$ emission peaks; b) Zn K-edge XAS spectrum (brown) and the reference spectrum collected at a synchrotron (yellow). (For interpretation of the references to colour in this figure legend, the reader is referred to the web version of this article.)

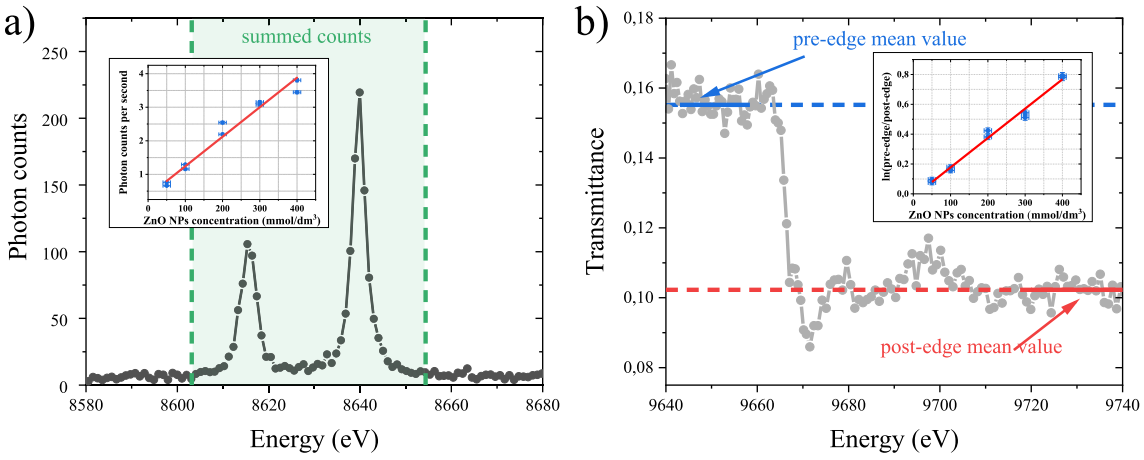

Fig. 4. a) XES spectrum measured for 200 mM ZnO NPs suspension. b) The spectrum of the X-ray beam transmitted through 200 mM ZnO NPs suspension. The green shaded area limited with dashed vertical lines in a) marks the region of summing photon counts. Blue and red solid lines in b) show the range of photon counts in the pre-edge and post-edge regions, respectively, which were averaged to evaluate the ZnO nanoparticle concentration. Dashed lines present extension of determined mean values to the whole range of the spectrum. Insets to Fig. a) and Fig. b) present concentration calibration curves for the XES and XAS measurements. (For interpretation of the references to colour in this figure legend, the reader is referred to the web version of this article.)

measurements were performed for a range of sample concentrations between 50 mmol/dm3 to 400 mmol/dm3. Obtained calibration curves for emission and absorption data are presented in Fig. 4a) and 4b) respectively as insets. As shown, acquired signals scale linearly with the sample concentration, and are the same for the top and bottom positions. The so-determined calibration curves were then used to scale measured XAS & XES intensities into the ZnO NPs concentration.

3.2. Dynamics of the sedimentation

The relative concentration changes of the ZnO NPs measured by tracking the X-ray emission and X-ray absorption over 88 min of data acquisition are presented in Fig. 5a) and 5b) respectively. The obtained emission and absorption observables were scaled to initial ZnO concentration of 200 mmol/dm^3 at the beginning of experiment. Experimental data obtained with applied mechanical stirring are marked with full blue circles for the measurement at the bottom of the polyimide capillary and full green circles when the X-ray beam was focused at the top of the container. The selected timestep value was a compromise between achieving sufficient time resolution of the measurement and providing good statistics of the detected X-ray signals. The value of the errors results from estimates of the statistical error and the uncertainty related to the calibration procedures. The performed test showed a stable signal during the whole experiment with applied stirrer regardless of the chosen capillary position.

Data collected for the unstirred sample at the top of the capillary (open green circles) show a significant drop in both emission and the absorption signal within tens of minutes of the measurement. An analogous increase of detected sample concentration was observed in the data collected at the bottom of the container (open blue circles). Both results strongly point to the occurrence of ZnO NPs agglomeration and sedimentation processes which were qualitatively and quantitatively analyzed by the present X-ray spectroscopy measurements. As depicted in Fig. 5, the sedimentation of the unstirred suspension follows an exponential trend and could be divided into three stages. Within the first 22 min of the experiment, both XAS and XES signals changed only a little compared to stirred sample. As the experiment went on, a rapid drop or rise (depending on whether the data were collected at the top or the bottom of the capillary) of the sample concentration occurred with the maximum sedimentation rate of about 2.5% of concentration change per minute after 40 min of the experiment. The maximum rate of sedimentation was obtained as the average of the 1st derivatives' inflection

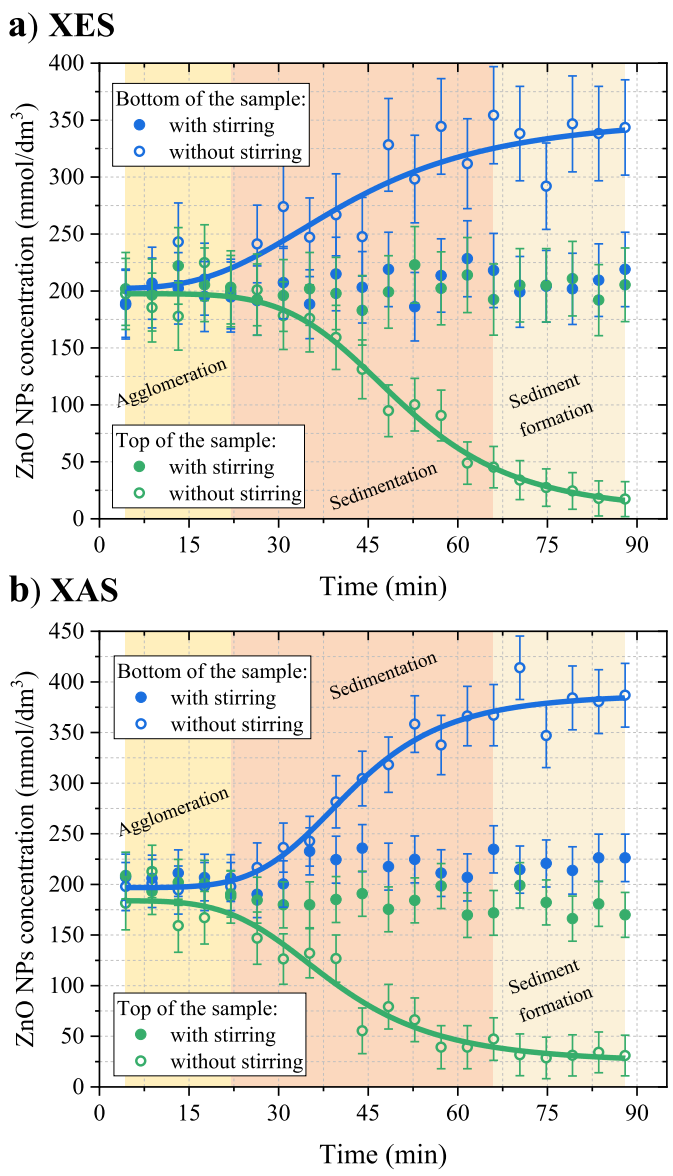

Fig. 5. Changes in sample concentration acquired from a) XES and b) XAS measurements over 88 min of data acquisition. Data obtained for the unstirred sample is marked as green (top) and blue (bottom) open circles with fitted sigmoid function (solid lines) indicating trends of the signal changes. Results obtained for stirred suspension at the top and bottom of the sample container are denoted with green and blue full circles respectively. Shaded areas from the left to right indicate phases of agglomeration, sedimentation and sediment formation. (For interpretation of the references to colour in this figure legend, the reader is referred to the web version of this article.)

points of change of sample concentration for XES and XAS. In the final stage of the sedimentation mechanism, the sediment formation phase started to occur as the monitored XES and XAS parameters reached a plateau. Since the sedimentation phenomenon takes place only when the particles are large enough for gravity to overcome other forces in the system and its speed increases with the increase of the particle size, the first phase is likely attributed to the formation of bigger particles through the agglomeration process, which then triggers stages of subsequent sedimentation and sediment formation when the growing clusters reach their critical size. Similar particle sedimentation mechanisms and time scales for the process were reported in other studies (both experimental measurements and theoretical calculations) with various types of the studied nanomaterials [38–40]. In particular, Azman et al. [38] reported a settlement time of about 45 min when studying the sedimentation velocity of copper nanoparticles in water at a comparable concentration. The conducted experiments, as in our case, showed very similar dynamics of NPs settlement. The process of the nanomaterials gathering into clusters triggering the sedimentation and occurring at a similar time scale of several dozen of minutes was also reported by Ming et al. [39] during the study of iron oxide nanorods and nanospheres. Nevertheless, it should be noted that obtained results were used to characterize the NPs system at given experimental conditions. Since the behavior of nanoparticle suspension would vary based on factors like the size, density, concentration, surface charge and fluid properties, more systematic studies would have to be performed to draw general observations that could be then transferred to a wider range of NPs suspensions. We should note that the quality of measurements' reproducibility can be evaluated for data presented for top and bottom positions and with applied stirring. In fact, these data confirm the relatively good reproducibility of the experiments. In addition, the performed calibration measurements showed a stable signal for each of the 10 samples (ZnO NPs suspensions at a concentration of 50, 100, 200, 300, 400 mM at two positions).

Comparison of two data sets obtained with and without the utilization of designed microliter stirrer setup clearly shows the influence of the application of continuous mixing on nanosuspension stability during long-time measurements. This is especially relevant because analysis of the nanomaterials in solution usually takes more time due to signal damping by the solvent.

4. Conclusions

In this article, we presented the newly developed microliter-stirred sample setup designed specifically to allow examination of down to 50 μL of liquid nanomaterial suspensions with continuous mixing of the sample during measurement preventing its agglomeration and subsequent sedimentation. The designed setup was manufactured with commercially available and relatively inexpensive components. Verification of its capabilities was performed with simultaneous XAS and XES spectroscopy using the laboratory-based double X-ray spectrometer. Results obtained for the stirred 200 mM ZnO nanoparticle suspension at the top and bottom of the sample container showed a stable signal over 1.5 h of data acquisition. On the other hand, in the case of experiments repeated for the unstirred ZnO NPs dispersion, visible changes in the sample concentration were observed within tens of minutes of the measurements due to the particle settlement at the bottom of the polyimide capillary. This enabled a qualitative and quantitative analysis of the sedimentation phenomenon observed for NPs suspended in water. Examination through XAS and XES revealed three distinguishable stages of NPs deposition process: initial agglomeration of ZnO NPs followed by subsequent sedimentation with the maximum rate of 2.5% concentration change per min at around 40 min and final phase that is sediment formation. The high quality of Zn Kα XES and Zn K-edge XAS spectra of ZnO nanoparticles indicates that the setup successfully be can used for long-time measurements of the liquid nanosuspensions in routine laboratory experiments. ZnO NPs are a widely studied class of nanomaterials with many potential applications including photocatalysis, heat transfer and biomedicine [41–44]. Examination of their properties in a liquid medium requires maintaining the physical stability of the dispersion. Concurrently, the presented studies can be further explored to a different Zn-based system like 0-dimensional quantum dots characterized by unique features that can be utilized in numerous applications like energy harvesting, display devices and sensors [45,46]. Further, the same strategy can be used in several other suspension-based 3d metals such as iron oxide NPs widely studied due to their magnetic properties [47,48] and plasmonic copper NPs utilized, for example in optoelectronic devices [49].

Declaration of Competing Interest

The authors declare that they have no known competing financial interests or personal relationships that could have appeared to influence the work reported in this paper.

Acknowledgment

This work was supported by the National Science Centre (Poland) under grant number 2020/37/B/ST3/00555.

References

[1] S.P. Gurway, P.R. Tete, Future of nanotechnology: an overview, AIP Conf. Proc. (2019) 2104, https://doi.org/10.1063/1.5100468.
[2] M. Nasrollahzadeh, S.M. Sajadi, M. Sajjadi, Z. Issaabadi, An Introduction to Nanotechnology, 1st ed, Elsevier Ltd., 2019, https://doi.org/10.1016/B978-0-12-813586-0.00001-8.
[3] M. Boholm, R. Arvidsson, A definition framework for the terms nanomaterial and nanoparticle, Nanoethics 10 (2016) 25–40, https://doi.org/10.1007/s11569-015-0249-7.
[4] S.K. Brar, M. Verma, Measurement of nanoparticles by light-scattering techniques, TrAC, Trends Anal. Chem. 30 (2011) 4–17, https://doi.org/10.1016/j.trac.2010.08.008.
[5] A.P. Defante, W.N. Vreeland, K.D. Benkstein, D.C. Ripple, Using image attributes to assure accurate particle size and count using nanoparticle tracking analysis, J. Pharm. Sci. 107 (2018) 1383–1391, https://doi.org/10.1016/j.xphs.2017.12.016.
[6] Q. Abbas, Understanding the UV-vis spectroscopy for nanoparticles, J. Nanomater. Mol. Nanotechnol. 8 (2019) 1–3, https://doi.org/10.4172/2324-8777.1000268.
[7] X. Tong, Z.M. Wang, Core/Shell Quantum Dots, Springer, 2020, https://doi.org/10.1007/978-3-030-46596-4.
[8] T. Guo, More power to X-rays: new developments in X-ray spectroscopy, Laser Photonics Rev. 3 (2009) 591–622, https://doi.org/10.1002/lpor.200810028.
[9] P. Zimmermann, S. Peredkov, P.M. Abdala, S. DeBeer, M. Tromp, C. Müller, J. A. van Bokhoven, Modern X-ray spectroscopy: XAS and XES in the laboratory, Coord. Chem. Rev. 423 (2020), 213466, https://doi.org/10.1016/j.ccr.2020.213466.
[10] W. Malzer, C. Schlesiger, B. Kanngießer, A century of laboratory X-ray absorption spectroscopy – a review and an optimistic outlook, Spectrochim. Acta - Part B At. Spectrosc. 177 (2021), https://doi.org/10.1016/j.sab.2021.106101.
[11] R. Ghosh Chaudhuri, S. Paria, Core/shell nanoparticles: classes, properties, synthesis mechanisms, characterization, and applications, Chem. Rev. 112 (2012) 2373–2433, https://doi.org/10.1021/cr100449n.
[12] D. Brabazon, E. Pellicer, F. Zivic, J. Sort, M.D. Baró, N. Grujovic, K.L. Choy, Commercialization of nanotechnologies-a case study approach, Commer. Nanotechnol. A Case Stud. Approach (2017) 1–315, https://doi.org/10.1007/978-3-319-56979-6.
[13] M. Sommer, F. Stenger, W. Peukert, N.J. Wagner, Agglomeration and breakage of nanoparticles in stirred media mills - a comparison of different methods and models, Chem. Eng. Sci. 61 (2006) 135–148, https://doi.org/10.1016/j.ces.2004.12.057.
[14] Agglomeration (Except in Polymer Science), IUPAC Compend. Chem. Terminol 1801, 2008, https://doi.org/10.1351/goldbook.a00182, 2014.
[15] S.C. Endres, L.C. Ciacchi, L. Mädler, A review of contact force models between nanoparticles in agglomerates, aggregates, and films, J. Aerosol Sci. 153 (2021), https://doi.org/10.1016/j.jaerosci.2020.105719.
[16] F. Henry, P. Marchal, J. Bouillard, A. Vignes, O. Dufaud, L. Perrin, The effect of agglomeration on the emission of particles from nanopowders flow, Chem. Eng. Trans. 31 (2013) 811–816, https://doi.org/10.3303/CET1331136.
[17] S. Ganguly, S. Chakraborty, Sedimentation of nanoparticles in nanoscale colloidal suspensions, Phys. Lett. Sect. A Gen. At. Solid State Phys. 375 (2011) 2394–2399, https://doi.org/10.1016/j.physleta.2011.04.018.
[18] X. Ma, Y. Zare, K.Y. Rhee, A two-step methodology to study the influence of aggregation/agglomeration of nanoparticles on Young's modulus of polymer nanocomposites, Nanoscale Res. Lett. 12 (2017) 0–6, https://doi.org/10.1186/s11671-017-2386-0.
[19] Y. Zare, K.Y. Rhee, D. Hui, Influences of nanoparticles aggregation/agglomeration on the interfacial/interphase and tensile properties of nanocomposites, Compos. Part B Eng. 122 (2017) 41–46, https://doi.org/10.1016/j.compositesb.2017.04.008.
[20] I. Lorite, J.J. Romero, J.F. Fernandez, Influence of the nanoparticles agglomeration state in the quantum-confinement effects: experimental evidences, AIP Adv. 5 (2015), https://doi.org/10.1063/1.4914107.
[21] J. Midelet, A.H. El-Sagheer, T. Brown, A.G. Kanaras, M.H.V. Werts, The sedimentation of colloidal nanoparticles in solution and its study using quantitative digital photography, Part. Part. Syst. Charact. 34 (2017), https://doi.org/10.1002/ppsc.201700095.
[22] Y.J. Yang, D.S. Corti, E.I. Franses, Use of close-packed vesicular dispersions to stabilize colloidal particle dispersions against sedimentation, Langmuir 31 (2015) 8802–8808, https://doi.org/10.1021/acs.langmuir.5b02133.
[23] Y.R. Jang, C.H. Ryu, J.H. Chu, J.B. Nam, H.S. Kim, Multiple intense pulsed light sintering of silane surface modified Cu oxide nanoparticle paste on Si wafer substrate for solar cell electrode, Thin Solid Films 722 (2021), 138577, https://doi.org/10.1016/j.tsf.2021.138577.
[24] M. Abdullah, S.R. Malik, M.H. Iqbal, M.M. Sajid, N.A. Shad, S.Z. Hussain, W. Razzaq, Y. Javed, Sedimentation and stabilization of nano-fluids with dispersant, Colloids Surf. A Physicochem. Eng. Asp. 554 (2018) 86–92, https://doi.org/10.1016/j.colsurfa.2018.06.030.
[25] F. Ordóñez, F. Chejne, E. Pabón, K. Cacua, Synthesis of ZrO2 nanoparticles and effect of surfactant on dispersion and stability, Ceram. Int. 46 (2020) 11970–11977, https://doi.org/10.1016/j.ceramint.2020.01.236.
[26] S. Yi, T. Babadagli, H. Li, Stabilization of nickel nanoparticle suspensions with the aid of polymer and surfactant: static bottle tests and dynamic micromodel flow tests, Pet. Sci. 17 (2020) 1014–1024, https://doi.org/10.1007/s12182-020-00433-1.
[27] S. Witharana, C. Hodges, D. Xu, X. Lai, Y. Ding, Aggregation and settling in aqueous polydisperse alumina nanoparticle suspensions, J. Nanopart. Res. 14 (2012) 1–19, https://doi.org/10.1007/s11051-012-0851-3.
[28] R.P. Singh, K. Sharma, K. Mausam, Dispersion and stability of metal oxide nanoparticles in aqueous suspension: a review, Mater. Today Proc. 26 (2019) 2021–2025, https://doi.org/10.1016/j.matpr.2020.02.439.
[29] A. Kumar, C.K. Dixit, Methods for characterization of nanoparticles, Adv. Nanomed. Deliv. Ther. Nucleic Acid (2017) 44–58, https://doi.org/10.1016/B978-0-08-100557-6.00003-1.
[30] H. Kamiya, Y. Otani, M. Fuji, M. Miyahara, Characteristics and Behavior of Nanoparticles and its Dispersion Systems, 2018, https://doi.org/10.1016/B978-0-444-64110-6.00003-2.
[31] S.U. Ilyas, R. Pendyala, N. Marneni, Preparation, sedimentation, and agglomeration of nanofluids, Chem. Eng. Technol. 37 (2014) 2011–2021, https://doi.org/10.1002/ceat.201400268.
[32] E.J. Cho, H. Holback, K.C. Liu, S.A. Abouelmagd, J. Park, Y. Yeo, Nanoparticle characterization: state of the art, challenges, and emerging technologies, Mol. Pharm. 10 (2013) 2093–2110, https://doi.org/10.1021/mp300697h.
[33] W. Błachucki, J. Czapla-Masztafiak, J. Sá, J. Szlachetko, A laboratory-based double X-ray spectrometer for simultaneous X-ray emission and X-ray absorption studies, J. Anal. At. Spectrom. 34 (2019) 1409–1415, https://doi.org/10.1039/c9ja00159j.
[34] J.L. Campbell, T. Papp, Widths of the atomic K-N7 levels, At. Data Nucl. Data Tables 77 (2001) 1–56, https://doi.org/10.1006/adnd.2000.0848.
[35] T.J. Penfold, J. Szlachetko, F.G. Santomauro, A. Britz, W. Gawelda, G. Doumy, A. M. March, S.H. Southworth, J. Rittmann, R. Abela, M. Chergui, C.J. Milne, Revealing hole trapping in zinc oxide nanoparticles by time-resolved X-ray spectroscopy, Nat. Commun. 9 (2018) 1–9, https://doi.org/10.1038/s41467-018-02870-4.
[36] T. Rossi, T.J. Penfold, M.H. Rittmann-Frank, M. Reinhard, J. Rittmann, C.N. Borca, D. Grolimund, C.J. Milne, M. Chergui, Characterizing the structure and defect concentration of ZnO nanoparticles in a colloidal solution, J. Phys. Chem. C 118 (2014) 19422–19430, https://doi.org/10.1021/jp505559u.
[37] A. Bhargava, C.Y. Chen, K.D. Finkelstein, M.J. Ward, R.D. Robinson, X-ray emission spectroscopy: an effective route to extract site occupation of cations, Phys. Chem. Chem. Phys. 20 (2018) 28990–29000, https://doi.org/10.1039/c8cp04628j.
[38] A. Azman, M.Z. Yusoff, M.Z. Hassan, H. Yazid, P. Gunnasegaran, K.C. Ng, Preliminary study to determine the maximum settling velocity and model parameter of Cu nanoparticle by settling method, IOP Conf, Ser. Mater. Sci. Eng. 785 (2020), https://doi.org/10.1088/1757-899X/785/1/012026.
[39] W.M. Ng, A. Katiyar, V. Mathivanan, X.J. Teng, S.S. Leong, S.C. Low, J.K. Lim, Sedimentation kinetics of magnetic nanoparticle clusters: iron oxide nanospheres vs nanorods, Langmuir 36 (2020) 5085–5095, https://doi.org/10.1021/acs.langmuir.0c00135.
[40] D.D. Liyanage, R.J.K.A. Thamali, A.A.K. Kumbalatara, J.A. Weliwita, S. Witharana, An analysis of nanoparticle settling times in liquids, J. Nanomater. (2016), https://doi.org/10.1155/2016/7061838 (2016).
[41] O. Marin, G. Grinblat, M. Tirado, D. Comedi, Nonmonotonic excitation power dependence of the UV photoluminescence rate from large ZnO nanoparticle assemblies, Nano-Struct. Nano-Obj. 26 (2021), 100734, https://doi.org/10.1016/j.nanoso.2021.100734.
[42] R.N. Radkar, B.A. Bhanvase, D.P. Barai, S.H. Sonawane, Intensified convective heat transfer using ZnO nanofluids in heat exchanger with helical coiled geometry at constant wall temperature, Mater. Sci. Energ. Technol. 2 (2019) 161–170, https://doi.org/10.1016/j.mset.2019.01.007.
[43] M.A. Borysiewicz, ZnO as a functional material, a review, Crystals 9 (2019), https://doi.org/10.3390/cryst9100505.
[44] M.H. Hidayat Chai, N. Amir, N. Yahya, I.M. Saaid, Characterization and colloidal stability of surface modified zinc oxide nanoparticle, J. Phys. Conf. Ser. (2018) 1123, https://doi.org/10.1088/1742-6596/1123/1/012007.
[45] D. Chen, A. Wang, M.A. Buntine, G. Jia, Recent advances in zinc-containing colloidal semiconductor nanocrystals for optoelectronic and energy conversion applications, ChemElectroChem. 6 (2019) 4709–4724, https://doi.org/10.1002/celc.201900838.
[46] M. Alizadeh-Ghodsi, M. Pourhassan-Moghaddam, A. Zavari-Nematabad, B. Walker, N. Annabi, A. Akbarzadeh, State-of-the-art and trends in synthesis, properties, and application of quantum dots-based nanomaterials, Part. Part. Syst. Charact. 36 (2019) 1–20, https://doi.org/10.1002/ppsc.201800302.
[47] S.M. Dadfar, K. Roemhild, N.I. Drude, S. von Stillfried, R. Knüchel, F. Kiessling, T. Lammers, Iron oxide nanoparticles: diagnostic, therapeutic and theranostic

applications, Adv. Drug Deliv. Rev. 138 (2019) 302–325, https://doi.org/10.1016/j.addr.2019.01.005.
[48] H. Shokrollahi, A review of the magnetic properties, synthesis methods and applications of maghemite, J. Magn. Magn. Mater. 426 (2017) 74–81, https://doi.org/10.1016/j.jmmm.2016.11.033.
[49] L. Wang, M. Hasanzadeh Kafshgari, M. Meunier, Optical properties and applications of Plasmonic-metal nanoparticles, Adv. Funct. Mater. (2020), https://doi.org/10.1002/adfm.202005400.